UC San Diego

UC San Diego Previously Published Works

Title

Small molecule NPT-440-1 inhibits ionic flux through Aβ1-42 pores: Implications for Alzheimer's disease therapeutics

Permalink

https://escholarship.org/uc/item/5808m3dk

Journal

Nanomedicine Nanotechnology Biology and Medicine, 12(8)

ISSN

1549-9634

Authors

Gillman, Alan L

Lee, Joon

Ramachandran, Srinivasan

et al.

Publication Date

2016-11-01

DOI

10.1016/j.nano.2016.06.001

Peer reviewed

eScholarship.org Powered by the California Digital Library
University of California

Author Manuscript

Author Manuscript

Author Manuscript

Author Manuscript

HHS Public Access

Author manuscript

Nanomedicine. Author manuscript; available in PMC 2017 November 01.

Published in final edited form as:

Nanomedicine. 2016 November ; 12(8): 2331–2340. doi:10.1016/j.nano.2016.06.001.

Small molecule NPT-440-1 inhibits ionic flux through $A\beta_{1-42}$ pores: implications for Alzheimer's disease therapeutics

Alan L. Gillman, PhD[a], **Joon Lee, CPhil**[b], **Srinivasan Ramachandran, PhD**[a,b], **Ricardo Capone, PhD**[c], **Tania Gonzalez, PhD**[c], **Wolf Wrasidlo, PhD**[c,d], **Eliezer Masliah, MD**[c,*], and **Ratnesh Lal, PhD**[a,b,**]

[a]Department of Bioengineering, University of California, San Diego, La Jolla, California 92093, United States

[b]Department of Mechanical and Aerospace Engineering, and Material Science and Engineering Program, University of California, San Diego, La Jolla, California 92093, United States

[c]Department of Neurosciences, University of California, San Diego, La Jolla, California 92093, United States

[d]Neuropore Therapies, Inc., 10835 Road to the Cure, Suite 210, San Diego, California, 92121, United States

Abstract

Increased levels of soluble amyloid-beta (Aβ) oligomers are suspected to underlie Alzheimer's disease (AD) pathophysiology. These oligomers have been shown to form multi-subunit Aβ pores in bilayers and induce uncontrolled, neurotoxic, ion flux, particularly calcium ions, across cellular membranes that might underlie cognitive impairment in AD. Small molecule interventions that modulate pore activity could effectively prevent or ameliorate their toxic activity. Here we examined the efficacy of a small molecule, NPT-440-1, on modulating amyloid pore permeability. Co-incubation of B103 rat neuronal cells with NPT-440-1 and $A\beta_{1-42}$ prevented calcium influx. In purified lipid bilayers, we show that a 10-15 min preincubation, prior to membrane introduction, was required to prevent conductance. Thioflavin-T and circular dichroism both suggested a reduction in $A\beta_{1-42}$ β-sheet content during this incubation period. Combined with previous studies on site-specific amino acid substitutions, these results suggest that pharmacological modulation of $A\beta_{1-42}$ could prevent amyloid pore-mediated AD pathogenesis.

GRAPHICAL ABSTRACT (TEXT)

Increased levels of soluble amyloid-beta (Aβ) oligomers are suspected to underlie Alzheimer's disease (AD) pathophysiology through the formation of uncontrolled multi-subunit Aβ pores in

*Corresponding Authors E.M.: Department of Neurosciences, University of California at San Diego (UCSD), MTF 348, 9500 Gilman Drive, MC 0624, La Jolla, CA 92093-0624, Tel: 858-534-8992, emasliah@ucsd.edu. **R.L.: Departments of Bioengineering and Mechanical & Aerospace Engineering, University of California at San Diego (UCSD), PFBH 217, 9500 Gilman Drive, MC 0412, La Jolla, CA 92093-0412, Tel: 858-822-0384, rlal@eng.ucsd.edu.

Publisher's Disclaimer: This is a PDF file of an unedited manuscript that has been accepted for publication. As a service to our customers we are providing this early version of the manuscript. The manuscript will undergo copyediting, typesetting, and review of the resulting proof before it is published in its final citable form. Please note that during the production process errors may be discovered which could affect the content, and all legal disclaimers that apply to the journal pertain.

Author Manuscript Author Manuscript Author Manuscript Author Manuscript

cellular membranes. In this study, the efficacy of small molecule NPT-440-1 modulation of $A\beta_{1-42}$ pore permeability was examined. We show that co-incubation of B103 rat neuronal cells with NPT-440-1 and $A\beta_{1-42}$ prevented calcium influx. In purified lipid bilayers, preincubation prior to membrane introduction was required to prevent conductance despite the presence of pore structures. The results point to compound-induced structural modulation leading to collapsed pores and suggest that pharmacological modulation of $A\beta_{1-42}$ could prevent AD pathogenesis.

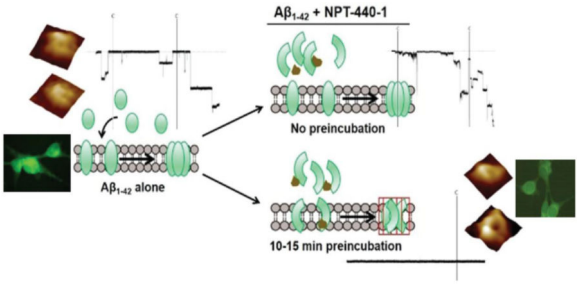

Keywords

Alzheimer's disease; Amyloid beta peptide; Amyloid pore; Small molecule; Calcium; Bilayer electrophysiology; Atomic force microscopy

BACKGROUND

Alzheimer's disease (AD) is one of the most devastating diseases associated with aging. It is diagnosed clinically by progressive cognitive and memory deficit, and only proven by the demonstration of Aβ plaques in the postmortem brains of AD patients. Brains of AD patients contain extracellular plaques and intracellular neurofibrillary tangles, as well as fewer synapses and neurons[1]. According to the amyloid cascade hypothesis, accumulation of amyloid-β (Aβ) peptides in the brain is the primary driver of pathogenesis, including synapse loss and neuronal cell death[2–6]. The plaques are composed of Aβ peptides aggregated into oligomeric and fibrillar species. The full-length $A\beta_{1-40/42}$ peptide is formed via APP cleavage by the action of β- and γ-secretases[3]. Although amyloid fibrils were initially believed to be the cytotoxic species in AD[7], increasing evidence indicates that intermediate Aβ oligomers are the toxic species[8–21]. A growing number of results suggest that Aβ oligomers disrupt cellular membranes by inserting to form pore structures[19,22–27]. More recent studies have pointed to a two-step mechanism of membrane disruption via membrane fragmentation and pore formation[20,21]. Pore activity has been observed for full length Aβs[17,18,22,23,28,29], Aβ fragments[30–37], and point substitutions[28,30,38]. Cytotoxicity results from an abrupt change in cell ionic concentration, in particular the increase in intracellular calcium levels, producing loss of cell homeostasis[39,40].

Although there have been several approaches for therapeutic intervention, there is currently no cure for AD[26,41,42]. These approaches have included the immunological clearing of Aβ plaques[26,43], but plaque removal did not prevent progressive neurodegeneration[26,44]. Other approaches focused on the processing of APP by secretase enzymes[26,41–43]. A widely used approach has been the use of β-secretase [β-site amyloid precursor protein (APP)-cleaving

Author Manuscript Author Manuscript Author Manuscript Author Manuscript

enzyme 1 (BACE1)] inhibitors to reduce $A\beta_{1\text{-}40/42}$ production[26,41,42]. Other approaches have included i) the reduction of $A\beta_{1\text{-}40/42}$ production by of γ-secretase inhibitors (GSIs)[26,45], ii) active and passive immunotherapy[41,43], and iii) current efforts to modulate γ-secretase activity by reducing the amount of $A\beta_{1\text{-}42}$ without reducing total Aβ protein load (GSMs)[46].

Here we discuss the biophysical properties and pore activity modulation mechanism of an aqueous soluble small-molecule compound. The compound, NPT-440-1, was designed as an aggregation blocker of $A\beta_{1\text{-}42}$. We show that the compound impedes $A\beta_{1\text{-}42}$ aggregation, normalizes intracellular calcium levels, and prevents the electrical activity of $A\beta_{1\text{-}42}$ pores. We suggest that a likely mechanism of action involves an NPT-440-1 induced conformational change leading to disruption of the β-barrel structure for membrane-embedded pore sections leading to non-conducting, and likely collapsed pores.

METHODS

$A\beta_{1–42}$ was purchased from Bachem (Torrance, CA), Anaspec (Fremont, CA), and American Peptide Company (Sunnyvale, CA). Phospholipids 1,2-dioleoyl-sn-glycero-3-phosphoserine (DOPS) and 1-palmitoyl-2-oleoyl-sn-glycero-3-phosphoethanolamine (POPE) were purchased from Avanti Polar Lipids (Alabaster, AL). The compound NPT-440-1 (Figure 1A), which upon initial solubilization in DMSO becomes water soluble, was provided by Neuropore Therapies, Inc. (San Diego, CA). All other chemicals were purchased from Sigma-Aldrich (St. Louis, MO).

Peptide and compound handling

For planar lipid bilayer (PLB) and Thioflavin-T (ThT) experiments, lyophilized $A\beta_{1–42}$ powder was dissolved in Milli-Q water to a concentration of 1 mg/mL (221.5 μM) before aliquoting for storage at −80 °C. Lyophilized NPT-440-1 powder was dissolved in DMSO to final concentration of 0.5 mM (for 10:1 peptide:compound condition) or 5 mM (1:1 condition) and stored at 4 °C for a maximum of 3 days. Aliquots were thawed only once.

SDS-PAGE Immunoblot

$A\beta_{1\text{-}42}$ was aggregated by incubating with different concentrations of NPT-440-1 at 37 °C for 16 h, followed by 6 h incubation at 56 °C[47,48]. Western blot analysis was performed as previously described by Masliah *et al.*[49] on a 4–12% SDS-polyacrylamide gel (Life Technologies, Carlsbad CA) and blotted onto a PVDF membrane. Blots were labeled with mouse monoclonal antibody 4G8 against $A\beta_{17–24}$ (dilution 1:1000) (Covance, Princeton NJ), followed by anti-mouse secondary antibodies (1:5000) (American Qualex, San Clemente CA).

Calcium assay

B103 rat neuronal cells were used for Fluo-4 MW Calcium imaging studies (Life Technologies, Carlsbad CA). Vehicle control consisted of cells in the absence of peptide and compound. Cells were co-incubated with 1 μM of oligomerized $A\beta_{1\text{-}42}$ and different concentrations of NPT-440-1 for 16 h prior to imaging.

Author Manuscript Author Manuscript Author Manuscript Author Manuscript

Planar lipid bilayer electrophysiolgy

Electrical recording were prepared using the "painted" technique[50]. 1:1 (w/w) solution of DOPS and POPE was prepared from stocks in chloroform, dried in a Rotavapor R-210 (Buchi), and resuspended in heptane to a total lipid concentration of 20 mg/mL. Bilayers were spontaneously formed from this solution by direct lipid apposition over ~250 μm diameter aperture in a Delrin septum (Warner Instruments, Delrin perfusion cup, volume 1 mL). As in previous studies, this membrane composition was shown to be stable for long recording times (4+ h)[36,51]. As electrolyte, we used 150 mM KCl, 10 mM HEPES (pH 7.4), and 1 mM $MgCl_2$ in both chambers. Control experiments establishing the stability of membranes formed with the addition of NPT-440-1 alone showed no effect on the stability of the bilayers.

Before performing any experiment, we verified that the bilayer was stable for several minutes with low conductance (<10 pS) across ±100 mV applied voltage and that the system capacitance was >110 pF and <200 pF. When these criteria were met, peptide was added directly to the cis (hot wire) side and stirred for 5 min. For the compound added trials, NPT-440-1 was added directly to the peptide aliquot at the desired molar ratio. The peptide/compound mixture was then either added immediately to the chamber or allowed to preincubate for 10-15 min prior to addition to the bilayer chamber. Peptide concentration in the bilayer chamber was 10 μM and final DMSO content was ~0.2%. Bilayer stability was monitored by periodic capacitance measurements throughout the course of the experiment.

All traces were recorded in voltage clamp mode using the 2 kHz built-in filter cutoff of the BC-535 amplifier (Warner Instruments, Hamden, CT). A sampling frequency of 15 kHz was used for all data acquisition. We used a custom-made LabVIEW program to record the current and Clampfit 10.2 (Molecular Devices, Sunnyvale, CA) to analyze traces. For representation in figures, we have filtered the recorded current versus time traces with a digital Gaussian low-pass filter with a cutoff frequency of 50 Hz.

Preparation of $A\beta_{1\text{-}42}$ and liposomes for AFM imaging

Powder form of $A\beta_{1\text{-}42}$ (Anaspec, CA) was first dissolved in 1% ammonium hydroxide and sonicated for 2 min in an ice bath to make sure the peptides were completely dissolved. The desired amount of peptide was aliquoted and lyophilized using a lyophilizer (FreeZone 2.5 Plus, Labconco, KS). The aliquots were stored at −80 °C for a maximum of 3 months prior to use. For AFM experiment, aliquoted peptides were taken from −80 °C, thawed and dissolved in 10 mM HEPES (1 mM $MgCl_2$, 150 mM KCl, pH = 7.4) buffer to make the concentration of 0.5 mg/ml. NPT-440-1 solution was added to make 10:1 peptide to compound molar ratio and incubated for 15 min before mixing with liposomes. For liposome preparation, 20 μL of DOPS and POPE lipids (5 mg/mL) in chloroform were mixed and chloroform was removed using a rotary evaporator yielding a lipid film. The dried lipid film was hydrated with 10 mM HEPES (1 mM $MgCl_2$, 150 mM KCl, pH = 7.4) buffer to a concentration of 0.5 mg/ml in a ~35 °C water bath for an hour with occasional vortexing. Finally, the solutions were sonicated for 5 min. The liposome solution was then mixed with $A\beta_{1\text{-}42}$ or $A\beta_{1\text{-}42}$ with NPT-440-1 (10:1 molar ratio) to make the peptide final concentration of 5.5 μM. For AFM imaging, 30 μl of the sample solution was deposited on

Author Manuscript Author Manuscript Author Manuscript Author Manuscript

freshly cleaved mica and incubated for ~10 min. Supported lipid bilayers are formed by vesicle rupture on mica surface during the incubation. Samples were rinsed with the buffer to remove unruptured liposomes still in solution. For fibrilization of $A\beta_{1\text{-}42}$, 66 μM of $A\beta_{1\text{-}42}$ was incubated with and without NPT-440-1 (10:1 peptide:compound molar ratio) at room temperature in solution for 40 h. 10 μl of the sample was deposited on freshly cleaved mica substrate for 10 min and dried using N_2 gas for AFM imaging.

AFM Imaging of $A\beta_{1\text{-}42}$ with NPT-440-1

Topographic images of $A\beta_{1\text{-}42}$ in solution and in DOPS/POPE (1:1) lipid membrane were acquired using a Multimode AFM equipped with a Nanoscope V controller (Bruker, Santa Barbara, CA). Silicon nitride cantilevers with a nominal spring constant of 0.4 N/m (SCANASYST-AIR, Bruker) for imaging in air and a spring constant of 0.08 N/m (TR400PSA, Asylum research) for imaging in fluid were employed using peak-force tapping mode. The Nanoscope software was used for analyzing imaging data.

Thioflavin-T fluorescence

Stock solution of 500 μM ThT in water was prepared and 2 μl were added to 100 μl HEPES (pH 7.4) buffer in 96-well white-walled plates (Nunclon, Denmark) to make 10 μM ThT solutions. For peptides, 221.5 μM stock aliquots were mixed to equilibrate peptide populations amongst the test conditions and then diluted to a concentration of 10 μM with 150 mM KCl, 10 mM HEPES (pH 7.4), 1 mM $MgCl_2$ buffer in the plate well. NPT-440-1 dissolved in DMSO was added to the desired final concentration before adding the peptide solution. Thioflavin-T fluorescence (450 nm excitation, 490 nm emission) was monitored every 5 min at 25° C for the indicated times using a SPECTRAmax Gemini EM fluorescent plate reader (Molecular Devices, Sunnyvale, CA). Samples were run in quadruplicates. $A\beta_{1\text{-}42}$ fluorescence intensity at each time point was set to 100% for sample comparison.

Circular dichroism (CD) spectroscopy

An Aviv410 CD spectrometer (Aviv Biomedical, Lakewood, NJ) was used to measure the differential absorbance of left- and right-handed circularly polarized light. Aliquots of 221.5 μM $A\beta_{1\text{-}42}$ were diluted in water to a final peptide concentration of 44.02 μM (0.199 mg/mL). NPT-440-1 powder was first solubilized in DMSO prior to addition to $A\beta_{1\text{-}42}$ at the desired molar ratio and subsequently diluted in water. To reduce the effect of DMSO on the CD spectrum, DMSO content was lowered as much as possible (final [DMSO] ≤0.12%). Samples were allowed to incubate 15 min prior to loading the cuvette. The spectra were recorded as the average of 9 scans over a wavelength range of 260–180 nm with 1 nm resolution and an averaging time of 0.5 sec. A 1 mm path length cuvette was used for all measurements. Background signal, using water (for $A\beta_{1\text{-}42}$ alone) or water + DMSO (for $A\beta_{1\text{-}42}$ + compound), was subtracted from the measurement and the observed signal, S in millidegrees, converted to the mean residue ellipicity ($[\theta]_{mrw}$) by the following equation[52,53]:

$$[\theta]_{mrw} = \frac{S \times MRW}{10 \times C_{mg/ml} \times L} \deg cm^2\ dmol^{-1}$$

Author Manuscript Author Manuscript Author Manuscript Author Manuscript

where L is path length (in cm), $C_{mg/ml}$ is the peptide concentration in mg/ml, and MRW is the mean residue weight (107.5 for $A\beta_{1-42}$).

RESULTS

NPT-440-1 inhibits aggregation $A\beta_{1-42}$ in solution

We first observed and validated the effect of NPT-440-1 on the aggregation of $A\beta_{1-42}$ in solution. Our SDS-PAGE data (Figure 1B/C) show that NPT-440-1 effectively reduces the formation of aggregates even at compound concentrations ten times smaller than that of the peptide. Co-incubation of NPT-440-1 with $A\beta_{1-42}$ reduced the formation of dimers, trimers, tetramers and higher order oligomers (Figure 1B). There is a concentration-dependent inhibition of overall oligomer formation, though this effect plateaus for the 2, 5, and 7 μM of NPT-440-1 samples (Figure 1C). We further studied the effect of NPT-440-1 on the aggregation of $A\beta_{1-42}$ in solution by AFM imaging. Figure 1D shows fibrils of $A\beta_{1-42}$ after 40 h incubation at room temperature in the buffer solution. The measured heights are in line with the typical height of fibrils ranging from 5–7 nm[54]. When $A\beta_{1-42}$ was incubated with NPT-440-1 at 10:1 molar ratio, we found reduction in the length of fibrils (Figure 1E) when compared to $A\beta_{1-42}$ alone (Figure 1D). This suggests NPT-440-1 disrupts and inhibits the aggregation and self-assembly behavior of $A\beta_{1-42}$ in solution.

NPT-440-1 rescues increased intracellular Ca^{2+} levels

The effectiveness of NPT-440-1 in maintaining normal intracellular Ca^{2+} levels in B103 rat neuronal cells during incubation with $A\beta_{1-42}$ was investigated (Figure 2). The presence of $A\beta_{1-42}$ induced a significant increase ($p < 0.01$) in intracellular Ca^{2+} (Figure 2B/D) whereas addition of NPT-440-1 (1:1 molar ratio) during incubation prevented this increase and Ca^{2+} levels remained at levels comparable to the vehicle control (Figure 2C/D). This result suggests that addition of NPT-440-1 prevents the $A\beta_{1-42}$ induced increase in intracellular Ca^{2+} ions.

Effect of NPT-440-1 on $A\beta_{1-42}$ pore conductivity and structure

The electrical activity of $A\beta_{1-42}$ pores in planar lipid membranes (DOPS/POPE 1:1) treated with NPT-440-1 was investigated via PLB experiments. $A\beta_{1-42}$ pore activity is seen as current steps in the tracing of ionic current passing through the lipid membrane (Figure 3A). Amyloid pores, unlike ion channels, are not regulated and do not exhibit integer values of a characteristic unitary conductance. Instead amyloid pores present with multilevel conductance values[18,23,25,30,31,33,36]. The current grows in a stepwise fashion showing pore forming activity, with newly formed or opened channels adding to the bulk activity of the membrane (Figure 3A). In all trials with the sole addition of $A\beta_{1-42}$ the overall current through the membrane kept increasing and eventually reached the saturation value of the amplifier. The effect of NPT-440-1 treatment was first examined at a 10:1 peptide:compound ratio. As shown by SDS-PAGE (Figure 1B/C) and AFM (Figure 1D/E), this ratio demonstrated an effect on $A\beta_{1-42}$ aggregation. When NPT-440-1 and $A\beta_{1-42}$ were preincubated for 10-15 min prior to introduction to the test chamber, all activity was prevented (Figure 3B). In 100% of trials ($n = 6$) this held true, with no deviation from baseline detected for at least 4 h of recording (Figure S1). To elucidate the effect of

Author Manuscript Author Manuscript Author Manuscript Author Manuscript

NPT-440-1 on $A\beta_{1-42}$ pore structure in the lipid membrane and to provide insight into the inhibitory mechanism against toxic ionic fluxes, AFM was utilized to visualize pore morphology. The inset images in Figure 3 show high-resolution AFM images of $A\beta_{1-42}$ pores in DOPS/POPE (1:1) lipid membranes with and without NPT-440-1 (see Figure S2 for full membrane images). Both samples show pore-like structures with similar properties. The height and diameter of $A\beta_{1-42}$ oligomers without NPT-440-1 were 1.6 ± 0.3 nm and 15.7 ± 4.0 nm (n = 70), respectively which corresponds with values reported in the literature[37,38]. Incubation of $A\beta_{1-42}$ with NPT-440-1 at 10:1 molar ratio shows similar height and diameter distribution of 1.5 ± 0.6 nm and 14.5 ± 3.9 nm respectively. The combined PLB/AFM data suggests that despite incubation with NPT-440-1, $A\beta_{1-42}$ is able to insert into the membrane and form pore structures, however these pores are non-conducting and thus non-cytotoxic in nature. In contrast to the results when $A\beta_{1-42}$ and NPT-440-1 are allowed prior incubation, simultaneous direct addition of NPT-440-1 and $A\beta_{1-42}$ to the test chamber showed no inhibitory effect on $A\beta_{1-42}$ pore activity with multilevel conductance events still clearly present (Figure 4A). This pattern held true even when the compound concentration was increased tenfold to a 1:1 ratio (Figure 4B), suggesting that incubation is the key step for pore disruption.

Reduction in β-sheet secondary structure

Since $A\beta_{1-42}$ aggregates are known to be rich in β-sheet secondary structure, we next studied the effect of NPT-440-1 on $A\beta_{1-42}$ secondary structure. As with the SDS-PAGE results, ThT fluorescence results indicate a concentration-dependent inhibitory effect of NPT-440-1 on $A\beta_{1-42}$ aggregation (Figure 6A). $A\beta_{1-42}$ initially exhibits the lowest average ThT signal (Figure 6A, left) with the 10:1 and 1:1 wells showing 101.3% and 107.9% comparative signal intensity respectively. When the error is accounted for, the initial intensities show no significant difference and demonstrate that there is no inherent quenching of the ThT signal by NPT-440-1. Despite starting with the lowest signal, after 15 min (Figure 6A, middle) $A\beta_{1-42}$ shows significantly more ThT fluorescence intensity than both the 10:1 ($p < 0.05$) and 1:1 ($p < 0.001$) NPT-440-1 treated samples. The effect of treatment with NPT-440-1 is further enhanced over time with significant reduction ($p < 0.001$) in the maximum ThT signal at both 10:1 and 1:1 $A\beta_{1-42}$:NPT-440-1 ratios after 42 h. By the 42 h point (Figure 6A, right) the 10:1 and 1:1 treated groups show 66.5% an 51.4% of the maximum $A\beta_{1-42}$ ThT intensity respectively. The CD spectrum of $A\beta_{1-42}$ showed β-sheet rich secondary structure with a characteristic negative peak near 218 nm (Figure 6B). The 10:1 NPT-440-1 treated $A\beta_{1-42}$ did not present a clean spectrum, due to interference by DMSO[53], particularly in the far UV region below 200nm. It is therefore difficult to make conclusions about wavelengths below 200nm. However, a clear upward shift is observed in the spectrum with a 15% reduction of the signal at 218 nm (red arrow in Figure 6B) suggesting a reduction in the peptide β-sheet character. Repeated trials consistently showed an upward shift in the $A\beta_{1-42}$ CD spectrum and reduction of the 218 nm signal by up to 67% as a result of preincubation with NPT-440-1 (Figure S3). This result correlates well with the reduction in ThT fluorescence intensity under identical treatment conditions, namely $A\beta_{1-42}$ with NPT-440-1 (10:1) after 15 min preincubation.

Author Manuscript Author Manuscript Author Manuscript Author Manuscript

DISCUSSION

We present data showing that 1) NPT-440-1 inhibits $A\beta_{1-42}$ aggregation (Figure 1), 2) incubation of NPT-440-1 with $A\beta_{1-42}$ effectively normalizes oligomer induced increases in intracellular Ca^{2+} levels (Figure 2) and eliminates $A\beta_{1-42}$ pore activity in DOPS/POPE (1:1) membranes (Figure 3). A detailed molecular explanation of pore modulation is difficult to determine because of the numerous potential mechanisms and missing knowledge about aspects of pore formation, structure, and conduction mechanisms. Possible mechanisms of NPT-440-1 activity modulation on $A\beta_{1-42}$ include: a) prevention of $A\beta_{1-42}$ binding and/or membrane insertion, b) prevention of pore assembly inside the membrane, or c) inducing a non-conducting/collapsed pore. These modulation events are not necessarily mutually exclusive and a combination of multiple effects is certainly possible. All of these potential events could be explained by an induced conformational change in $A\beta_{1-42}$ oligomer structure.

The SDS-PAGE data (Figure 1) indicates that NPT-440-1 inhibits aggregation of $A\beta_{1-42}$ monomers and small oligomers into intermediate oligomers, which are currently thought to be the most toxic species. These toxic oligomers induce membrane deficits, or pores, which have been shown to lead to increases in intracellular calcium levels. Prevention of intermediate oligomer formation should lessen, or prevent, the influx of calcium. We find that incubation of oligomerized $A\beta_{1-42}$ with B103 rat neuronal cells leads to a significant increase ($p < 0.01$) in intracellular calcium (Figure 2B) when compared to vehicle (Figure 2A). This effect is prevented by 1:1 co-incubation of NPT-440-1 and $A\beta_{1-42}$, significantly reducing ($p < 0.001$) intracellular calcium levels when compared to the $A\beta_{1-42}$ only treated case (Figure 2C). Treatment with NPT-440-1 prevents the amyloid induced membrane disturbances and leads to normalized intracellular calcium levels that are comparable to vehicle control (Figure 2D).

Further study will be needed to elucidate in detail if there is a linear relationship between the effects of NPT-440-1 oligomer formation and the functional effects observed in the in vitro system. However, based on previous studies, even modest reduction on peptide aggregation (30%) could have dramatic effects on overall oligomer formation and toxicity[55]. The mechanisms are not completely clear and may have to do with the large variability and complex kinetics of Aβ oligomer formation[56], as we have previously shown utilizing molecular modeling techniques[55]. Under these conditions, a 50% reduction in oligomer formation could be sufficient to have considerable effects in fully suppressing Aβ toxicity.

Given the success of NPT-440-1 normalizing cellular calcium levels, we decided to look specifically at the ability of the compound to prevent pore formation in lipid bilayers. A mixture of phosphoethanolamine (PE) and phosphoserine (PS) lipid headgroups were chosen as these are dominant lipid components in the brains of the elderly[57], and these levels have been found to change in AD brains[58]. Using PLB recordings we monitored the ionic current crossing a model membrane system. PLB provides true single channel resolution of conduction through the test membrane. As expected, $A\beta_{1-42}$ demonstrated multilevel conductance events in the DOPS/POPE bilayer (Figure 3A) and annular pore structures are observed in the membrane by high-resolution AFM (Figure 3A, inset). Fluctuations in the

Author Manuscript Author Manuscript Author Manuscript Author Manuscript

recorded current represent ionic conductance across the membrane with step events indicative of a pore opening/closing. As seen in Figure 3A, these pores can be open simultaneously and the contribution from individual pores stack, growing the bulk ionic conductance across the membrane. Given sufficient time, $A\beta_{1-42}$ activity leads to the saturation of the current amplifier. An effective inhibitor is expected to prevent this activity from occurring.

When allowed to preincubate with $A\beta_{1-42}$ for 10-15 min prior to addition to the test chamber, NPT-440-1 successfully inhibited $A\beta_{1-42}$ pore activity (Figure 3B) despite the presence of pore structures in the membrane (Figure 3B, inset) similar to those found in the untreated case. The presence of non-conducting pore structures implies a structural change within the membrane-embedded region of the pore inhibiting toxic ionic flux through the pore. This behavior was seen reliably in all experiments with preincubation (n = 6) at a 10:1 peptide:compound ratio. However, simultaneous addition of $A\beta_{1-42}$ and NPT-440-1 to the test chamber, with no preicubation, showed no tangible effect on ionic conductance when compared to $A\beta_{1-42}$ alone for both 10:1 (Figure 4A) and 1:1 (Figure 4B) peptide:compound ratios. In both cases the pore forming activity of $A\beta_{1-42}$ demonstrated multilevel conductance steps with periods of spike and burst activities that are also commonly seen in recordings where $A\beta_{1-42}$ alone was added. As with the untreated case, the activity led to saturation of the current amplifier.

The results without preincubation are clearly not the result of insufficient NPT-440-1 concentration since activity was still seen with ten times more compound than was effective in the preincubated case shown in Figure 3B. From this result it is apparent that a conformational change in the peptide must occur during the preincubation period, prior to the introduction of $A\beta_{1-42}$ to the bilayer. $A\beta_{1-42}$ pores are composed of variable number of mobile subunits (small oligomers) that must find each other and assemble within the membrane[33] (Figure 5A). The variable nature of these pore assemblies is thought to lead to the heterogenous conductance levels that are seen in PLB recordings of all amyloid peptides tested to date[18]. The need for preincubation suggests that at least a minor fraction of these $A\beta_{1-42}$ subunits insert quickly when exposed to the DOPS/POPE lipid bilayer present in the recording chamber, where they are likely shielded from the effect of NPT-440-1 and remain free to assemble into conducting pores (Figure 5B). Preincubation of $A\beta_{1-42}$ with NPT-440-1 appears to allow sufficient time for conformational change to be induced prior to binding and shielding on the membrane (Figure 5C). The NPT-440-1 induced conformational change may prevent membrane insertion, pore formation, or induce a collapsed pore (Figure 5C), all of which would lead to no electrical activity being seen in the PLB recordings. Our structural studies with high-resolution AFM (Figure 3B, inset) point toward the formation of collapsed, non-conducting pores as a result of incubation with NPT-440-1.

Numerous MD simulations of Aβ pores suggest that β-barrel structures for the intramembrane region of the pore would be stable[33,35,37,38,51], while a recent study by Bhowmik et al.[59] provides experimental evidence for β-sheet rich Aβ pores in the membrane. We have previously shown that $A\beta_{1-42}$ containing a point substituted proline (F19P) showed a normal pore structure by AFM but did not demonstrate ionic conductance

Author Manuscript Author Manuscript Author Manuscript Author Manuscript

in PLB, while the MD suggested a stable collapsed pore[30,38,51]. The chemical structure of proline introduces a “kink” in the peptide's secondary structure, which is known to disrupt β-sheet formation. The MD simulations of F19P $A\beta_{1-42}$ barrel structure showed that β-sheet destabilization led the highly charged N-terminal regions to bind at the peptide mouth and collapsed the pore[30,38]. Our current PLB and AFM data appear remarkably similar to that of F19P[38,51] and suggest that NPT-440-1 likely inhibits ionic conductance through a similar mechanism, namely by reducing or breaking the β-sheet secondary structure within $A\beta_{1-42}$ pore forming oligomers.

Based on these studies, we investigated whether NPT-440-1 had any effect on the β-sheet content of $A\beta_{1-42}$. The ThT results show clear reduction of the β-sheet secondary structure of $A\beta_{1-42}$ when co-incubated with NPT-440-1. As with the SDS-PAGE data, the ThT fluorescence results indicate a concentration-dependent inhibitory effect of NPT-440-1 on $A\beta_{1-42}$ aggregation (Figure 6A). It is interesting to note that while aggregation was monitored via ThT fluorescence over the course of 42 h, a clear and significant ($p < 0.05$) effect of treatment with the compound was observed within the first 15 min at the same 10:1 ratio that prevented ionic conductance in PLB. Since ThT primarily detects β-sheet structures[60], these results suggest that NPT-440-1 may inhibit $A\beta_{1-42}$ aggregation and formation into β-sheet containing pore structures in the membrane.

This theory is bolstered when carefully analyzing the CD data (Figure 6B). An upward shift is seen in the NPT-440-1 treated spectrum with a 15% reduction at 218 nm (red arrow in Figure 6B), after 15 min of incubation, for the compound treated peptide when compared to the compound free, $A\beta_{1-42}$ only, case. The upward shift of a peak region in the range of our observed signal strength is a known indicator of a reduction in the β-sheet character of peptides[52]. While inconclusive on its own, when combined with our ThT, PLB, and AFM data, these results are highly suggestive of disruption of the β-sheet secondary structure in $A\beta_{1-42}$. Taken together, the studies suggest that β-sheet structure is necessary for toxic conductance through Aβ channels.

We demonstrate that NPT-440-1 reduces aggregation of $A\beta_{1-42}$ into intermediate oligomers that are implicated in cytotoxicity. Treatment of B103 rat neuronal cells shows that NPT-440-1 prevents the increases in intracellular calcium levels induced by $A\beta_{1-42}$. PLB recordings showed that preincubation of NPT-440-1 with $A\beta_{1-42}$ effectively eliminated cytotoxic ionic flux across the bilayer while introduction to the bilayer prior to preincubation showed no effect. Investigation of the peptide secondary structure, using ThT fluorescence and CD spectroscopy, suggests that NPT-440-1 reduces the β-sheet content of $A\beta_{1-42}$. We propose that NPT-440-1 and other pharmacologic agents that structurally target amyloid peptides could prove effective in slowing or preventing the progression of AD and other amyloid mediated neurodegenerative diseases and should be investigated further.

Supplementary Material

Refer to Web version on PubMed Central for supplementary material.

Author Manuscript Author Manuscript Author Manuscript Author Manuscript

ACKNOWLEDGMENTS

The authors would like to thank Neuropore Therapies Inc. for generously providing NPT-440-1. Thanks are also given to the UCSD Biophysics Instrumentation Facility for the use of the Aviv410 CD spectrometer used in this study.

Funding Source Information: Work supported by National Institutes of Health Grants R01 AG028709 (R.L.) and R37 AG18440 (E.M.)

REFERENCES

(1). Di Paolo G, Kim T-W. Linking lipids to Alzheimer's disease: cholesterol and beyond. Nat. Rev. Neurosci. 2011; 12:284–296. [PubMed: 21448224]

(2). Tanzi RE, Bertram L. Twenty Years of the Alzheimer's Disease Amyloid Hypothesis-A Genetic Perspective. Cell. 2005; 120:545–555. [PubMed: 15734686]

(3). Iversen LL, Mortishiresmith RJ, Pollack SJ, Shearman MS. The Toxicity in-Vitro of β-Amyloid Protein. Biochem. J. 1995; 311:1–16. [PubMed: 7575439]

(4). Jakob-Roetne R, Jacobsen H. Alzheimer's disease: from pathology to therapeutic approaches. Angew. Chem. Int. Ed. Engl. 2009; 48:3030–3059. [PubMed: 19330877]

(5). Hardy J, Selkoe DJ. The amyloid hypothesis of Alzheimer's disease: progress and problems on the road to therapeutics. Science. 2002; 297:353–356. [PubMed: 12130773]

(6). Hardy J, Higgins G. Alzheimer's disease: the amyloid cascade hypothesis. Science. 1992; 256:184–185. [PubMed: 1566067]

(7). Sipe JD, Cohen AS. Review: history of the amyloid fibril. J. Struct. Biol. 2000; 130:88–98. [PubMed: 10940217]

(8). Bucciantini M, Giannoni E, Chiti F, Baroni F, Formigli L, Zurdo J, Taddei N, Ramponi G, Dobson CM, Stefani M. Inherent toxicity of aggregates implies a common mechanism for protein misfolding diseases. Nature. 2002; 416:507–511. [PubMed: 11932737]

(9). Nussbaum JM, Schilling S, Cynis H, Silva A, Swanson E, Wangsanut T, Tayler K, Wiltgen B, Hatami A, Rönicke R, Reymann K, Hutter-Paier B, Alexandru A, Jagla W, Graubner S, Glabe CG, Demuth H-U, Bloom GS. Prion-like behaviour and tau-dependent cytotoxicity of pyroglutamylated amyloid-β. Nature. 2012; 485:651–655. [PubMed: 22660329]

(10). Stroud JC, Liu C, Teng PK, Eisenberg D. Toxic fibrillar oligomers of amyloid-β have cross-β structure. Proc. Natl. Acad. Sci. 2012; 109:7717–7722. [PubMed: 22547798]

(11). Bernstein SL, Dupuis NF, Lazo ND, Wyttenbach T, Condron MM, Bitan G, Teplow DB, Shea J-E, Ruotolo BT, Robinson CV, Bowers MT. Amyloid-β protein oligomerization and the importance of tetramers and dodecamers in the aetiology of Alzheimer's disease. Nat. Chem. 2009; 1:326–331. [PubMed: 20703363]

(12). Chiti F, Dobson CM. Protein misfolding, functional amyloid, and human disease. Annu. Rev. Biochem. 2006; 75:333–366. [PubMed: 16756495]

(13). Eisenberg D, Jucker M. The amyloid state of proteins in human diseases. Cell. 2012; 148:1188–1203. [PubMed: 22424229]

(14). Jang H, Zheng J, Lal R, Nussinov R. New structures help the modeling of toxic amyloid β ion channels. Trends Biochem. Sci. 2008; 33:91–100. [PubMed: 18182298]

(15). Lashuel HA, Hartley D, Petre BM, Walz T, Lansbury PT. Neurodegenerative disease: amyloid pores from pathogenic mutations. Nature. 2002; 418:291.

(16). Lashuel HA, Lansbury PT. Are amyloid diseases caused by protein aggregates that mimic bacterial pore-forming toxins? Q. Rev. Biophys. 2006; 39:167–201. [PubMed: 16978447]

(17). Lin H, Bhatia R, Lal R. Amyloid β protein forms ion channels: implications for Alzheimer's disease pathophysiology. FASEB J. 2001; 15:2433–2444. [PubMed: 11689468]

(18). Quist A, Doudevski I, Lin H, Azimova R, Ng D, Frangione B, Kagan B, Ghiso J, Lal R. Amyloid ion channels: a common structural link for protein-misfolding disease. Proc. Natl. Acad. Sci. U. S. A. 2005; 102:10427–10432. [PubMed: 16020533]

Author Manuscript Author Manuscript Author Manuscript Author Manuscript

(19). Kagan BL, Hirakura Y, Azimov R, Azimova R, Lin MC. The channel hypothesis of Alzheimer's disease: Current status. Peptides. 2002; 23:1311–1315. [PubMed: 12128087]

(20). Sciacca MFM, Kotler SA, Brender JR, Chen J, Lee D, Ramamoorthy A. Two-step mechanism of membrane disruption by Aβ through membrane fragmentation and pore formation. Biophys. J. 2012; 103:702–710. [PubMed: 22947931]

(21). Kotler SA, Walsh P, Brender JR, Ramamoorthy A. Differences between amyloid-β aggregation in solution and on the membrane: insights into elucidation of the mechanistic details of Alzheimer's disease. Chem. Soc. Rev. 2014; 43:6692–6700. [PubMed: 24464312]

(22). Arispe N, Rojas E, Pollard HB. Alzheimer disease amyloid β protein forms calcium channels in bilayer membranes: blockade by tromethamine and aluminum. Proc. Natl. Acad. Sci. U. S. A. 1993; 90:567–571. [PubMed: 8380642]

(23). Arispe N, Pollard HB, Rojas E. Giant multilevel cation channels formed by Alzheimer disease amyloid β-protein [AβP-(1-40)] in bilayer membranes. Proc. Natl. Acad. Sci. U. S. A. 1993; 90:10573–10577. [PubMed: 7504270]

(24). Capone RF, Quiroz FG, Prangkio P, Saluja I, Sauer AM, Bautista MR, Turner RS, Yang J, Mayer M. Amyloid-β Ion Channels in Artificial Lipid Bilayers and Neuronal Cells. Resolving a Controversy. Biophys. J. 2009; 16:1–13.

(25). Kagan BL, Azimov R, Azimova R. Amyloid peptide channels. J. Membr. Biol. 2004; 202:1–10. [PubMed: 15702375]

(26). Jang H, Connelly L, Arce FT, Ramachandran S, Lal R, Kagan BL, Nussinov R. Alzheimer's disease: which type of amyloid-preventing drug agents to employ? Phys. Chem. Chem. Phys. 2013; 15:8868–8877. [PubMed: 23450150]

(27). Jang H, Connelly L, Teran Arce F, Ramachandran S, Kagan BL, Lal R, Nussinov R. Mechanisms for the insertion of toxic, fibril-like β-amyloid oligomers into the membrane. J. Chem. Theory Comput. 2013; 9:822–833. [PubMed: 23316126]

(28). Connelly L, Jang H, Teran Arce F, Capone R, Kotler SA, Ramachandran S, Kagan BL, Nussinov R, Lal R. Atomic force microscopy and MD simulations reveal pore-like structures of all-D-enantiomer of Alzheimer's β-amyloid peptide: relevance to the ion channel mechanism of AD pathology. J. Phys. Chem. B. 2012; 116:1728–1735. [PubMed: 22217000]

(29). Capone R, Jang H, Kotler S. a. Connelly L, Teran Arce F, Ramachandran S, Kagan BL, Nussinov R, Lal R. All-d-enantiomer of β-amyloid peptide forms ion channels in lipid bilayers. J. Chem. Theory Comput. 2012; 8:1143–1152. [PubMed: 22423218]

(30). Jang H, Arce FT, Ramachandran S, Capone R, Azimova R, Kagan BL, Nussinov R, Lal R. Truncated β-amyloid peptide channels provide an alternative mechanism for Alzheimer's Disease and Down syndrome. Proc. Natl. Acad. Sci. U. S. A. 2010; 107:6538–6543. [PubMed: 20308552]

(31). Lin MA, Kagan BL. Electrophysiologic properties of channels induced by Aβ25–35 in planar lipid bilayers. Peptides. 2002; 23:1215–1228. [PubMed: 12128079]

(32). Arce FT, Jang H, Ramachandran S, Landon PB, Nussinov R, Lal R. Polymorphism of amyloid β peptide in different environments: implications for membrane insertion and pore formation. Soft Matter. 2011; 7:5267–5273. [PubMed: 21918653]

(33). Jang H, Arce FT, Capone R, Ramachandran S, Lal R, Nussinov R. Misfolded amyloid ion channels present mobile β-sheet subunits in contrast to conventional ion channels. Biophys. J. 2009; 97:3029–3037. [PubMed: 19948133]

(34). Jang H, Teran Arce F, Ramachandran S, Capone R, Lal R, Nussinov R. Structural convergence among diverse, toxic β-sheet ion channels. J. Phys. Chem. B. 2010; 114:9445–9451. [PubMed: 20608696]

(35). Jang H, Arce FT, Ramachandran S, Capone R, Lal R, Nussinov R. β-Barrel Topology of Alzheimer's β-Amyloid Ion Channels. J. Mol. Biol. 2010; 404:917–934. [PubMed: 20970427]

(36). Gillman AL, Jang H, Lee J, Ramachandran S, Kagan BL, Nussinov R, Teran Arce F. Activity and architecture of pyroglutamate-modified amyloid-β (AβpE3-42) pores. J. Phys. Chem. B. 2014; 118:7335–7344. [PubMed: 24922585]

Author Manuscript Author Manuscript Author Manuscript Author Manuscript

(37). Lee J, Gillman AL, Jang H, Ramachandran S, Kagan BL, Nussinov R, Teran Arce F. Role of the fast kinetics of pyroglutamate-modified amyloid-β oligomers in membrane binding and membrane permeability. Biochemistry. 2014; 53:4704–4714. [PubMed: 24950761]

(38). Connelly L, Jang H, Teran Arce F, Ramachandran S, Kagan BL, Nussinov R, Lal R. Effects of point substitutions on the structure of toxic Alzheimer's β-amyloid channels: Atomic force microscopy and molecular dynamics simulations. Biochemistry. 2012; 51:3031–3038. [PubMed: 22413858]

(39). Mattson MP, Cheng B, Davis D, Bryant K, Lieberburg I, Rydel RE. β-Amyloid peptides destabilize calcium homeostasis and render human cortical neurons vulnerable to excitotoxicity. J. Neurosci. 1992; 12:376–389. [PubMed: 1346802]

(40). Loo DT, Copani A, Pike CJ, Whittemore ER, Walencewicz AJ, Cotman CW. Apoptosis is induced by β-amyloid in cultured central nervous system neurons. Proc. Natl. Acad. Sci. U. S. A. 1993; 90:7951–7955. [PubMed: 8367446]

(41). Chiang K, Koo EH. Emerging therapeutics for Alzheimer's disease. Annu. Rev. Pharmacol. Toxicol. 2014; 54:381–405. [PubMed: 24392696]

(42). Teich AF, Arancio O. Is the Amyloid Hypothesis of Alzheimer's disease therapeutically relevant? Biochem. J. 2012; 446:165–177. [PubMed: 22891628]

(43). Citron M. Strategies for disease modification in Alzheimer's disease. Nat. Rev. Neurosci. 2004; 5:677–685. [PubMed: 15322526]

(44). Holmes C, Boche D, Wilkinson D, Yadegarfar G, Hopkins V, Bayer A, Jones RW, Bullock R, Love S, Neal JW, Zotova E, Nicoll JA. Long-term effects of Aβ42 immunisation in Alzheimer's disease: follow-up of a randomised, placebo-controlled phase I trial. Lancet. 2008; 372:216–223. [PubMed: 18640458]

(45). Bateman RJ, Siemers ER, Mawuenyega KG, Wen G, Browning KR, Sigurdson WC, Yarasheski KE, Friedrich SW, DeMattos RB, May PC, Paul SM, Holtzman DM. A γ-secretase inhibitor decreases amyloid-β production in the central nervous system. Ann. Neurol. 2009; 66:48–54. [PubMed: 19360898]

(46). Dimitrov M, Alattia J-R, Lemmin T, Lehal R, Fligier A, Houacine J, Hussain I, Radtke F, Dal Peraro M, Beher D, Fraering PC. Alzheimer's disease mutations in APP but not γ-secretase modulators affect epsilon-cleavage-dependent AICD production. Nat. Commun. 2013; 4:2246. [PubMed: 23907250]

(47). Spencer B, Michael S, Shen J, Kosberg K, Rockenstein E, Patrick C, Adame A, Masliah E. Lentivirus mediated delivery of neurosin promotes clearance of wild-type α-synuclein and reduces the pathology in an α-synuclein model of LBD. Mol. Ther. 2013; 21:31–41. [PubMed: 22508489]

(48). Spencer B, Emadi S, Desplats P, Eleuteri S, Michael S, Kosberg K, Shen J, Rockenstein E, Patrick C, Adame A, Gonzalez T, Sierks M, Masliah E. ESCRT-mediated uptake and degradation of brain-targeted α-synuclein single chain antibody attenuates neuronal degeneration in vivo. Mol. Ther. 2014; 22:1753–1767. [PubMed: 25008355]

(49). Masliah E, Rockenstein E, Veinbergs I, Mallory M, Hashimoto M, Takeda A, Sagara Y, Sisk A, Mucke L. Dopaminergic loss and inclusion body formation in alpha-synuclein mice: implications for neurodegenerative disorders. Science. 2000; 287:1265–1269. [PubMed: 10678833]

(50). Mueller P, Rudin DO, Tien HT, Wescott WC. Reconstitution of cell membrane structure in vitro and its transformation into an excitable system. Nature. 1962; 194:979–980. [PubMed: 14476933]

(51). Capone R, Jang H, Kotler S. a. Kagan BL, Nussinov R, Lal R. Probing structural features of Alzheimers amyloid-β pores in bilayers using site-specific amino acid substitutions. Biochemistry. 2012; 51:776–785. [PubMed: 22242635]

(52). Greenfield NJ. Using circular dichroism spectra to estimate protein secondary structure. Nat. Protoc. 2006; 1:2876–2890. [PubMed: 17406547]

(53). Martin SR, Schilstra MJ. Circular dichroism and its application to the study of biomolecules. Methods Cell Biol. 2008; 84:263–293. [PubMed: 17964935]

(54). Parbhu A, Lin H, Thimm J, Lal R. Imaging real-time aggregation of amyloid beta protein (1-42) by atomic force microscopy. Neurosci. Res. 2002; 23:1265–1270.

Author Manuscript Author Manuscript Author Manuscript Author Manuscript

(55). Tsigelny IF, Sharikov Y, Kouznetsova VL, Greenberg JP, Wrasidlo W, Gonzalez T, Desplats P, Michael SE, Trejo-Morales M, Overk CR, Masliah E. Structural diversity of Alzheimer's disease amyloid-β dimers and their role in oligomerization and fibril formation. J. Alzheimers. Dis. 2014; 39:583–600. [PubMed: 24240640]

(56). Jan A, Adolfsson O, Allaman I, Buccarello A-L, Magistretti PJ, Pfeifer A, Muhs A, Lashuel HA. Abeta42 neurotoxicity is mediated by ongoing nucleated polymerization process rather than by discrete Abeta42 species. J. Biol. Chem. 2011; 286:8585–8596. [PubMed: 21156804]

(57). Soderberg M, Edlund C, Alafuzoff I, Kristensson K, Dallner G. Lipid composition in different regions of the brain in Alzheimer's disease/senile dementia of Alzheimer's type. J. Neurochem. 1992; 59:1646–1653. [PubMed: 1402910]

(58). Wells K, Farooqui AA, Liss L, Horrocks LA. Neural membrane phospholipids in alzheimer disease. Neurochem. Res. 1995; 20:1329–1333. [PubMed: 8786819]

(59). Bhowmik D, Mote KR, MacLaughlin CM, Biswas N, Chandra B, Basu JK, Walker GC, Madhu PK, Maiti S. Cell-Membrane-Mimicking Lipid-Coated Nanoparticles Confer Raman Enhancement to Membrane Proteins and Reveal Membrane-Attached Amyloid-β Conformation. ACS Nano. 2015; 9:9070–9077. [PubMed: 26391443]

(60). Biancalana M, Koide S. Molecular mechanism of Thioflavin-T binding to amyloid fibrils. Biochim. Biophys. Acta - Proteins Proteomics. 2010; 1804:1405–1412.

Author Manuscript Author Manuscript Author Manuscript Author Manuscript

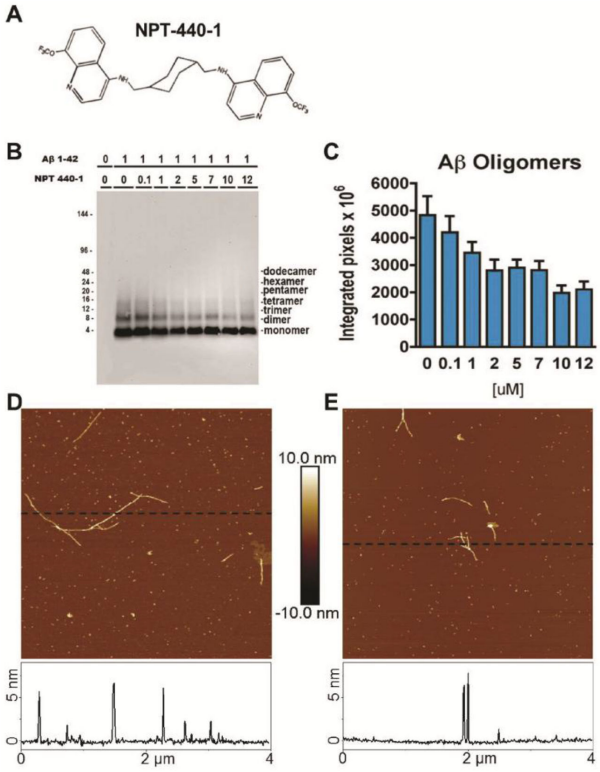

FIGURE 1. NPT-440-1 reduces $A\beta_{1-42}$ aggregation

A) Chemical structure of NPT-440-1. 1 μM $A\beta_{1-42}$ was allowed to aggregate during incubation with NPT-440-1 at different concentrations (0.1–12 μM) in a cell free system. NPT-440-1 reduced the formation of $A\beta_{1-42}$ dimers, trimers, tetramers and higher order oligomers. Aggregation reduction is dose dependent, but response is seen in other tests at 10:1 peptide:compound ratio. **B)** Western blot labeled with mouse monoclonal anti- $A\beta_{1-42}$ (1:1000), followed by anti-mouse secondary antibodies (1:5000). **C)** Quantification of gel in B. **D–E)** AFM images of $A\beta_{1-42}$ with and without NPT-440-1 on mica after 40 h. **D)** $A\beta_{1-42}$ alone shows long fibrils with small oligomers. **E)** $A\beta_{1-42}$ with NPT440-1 (10:1 molar ratio) shows shorter fibrils with small oligomers. Height section profiles at the dotted line are plotted below. Images are 4 μm × 4 μm.

Author Manuscript Author Manuscript Author Manuscript Author Manuscript

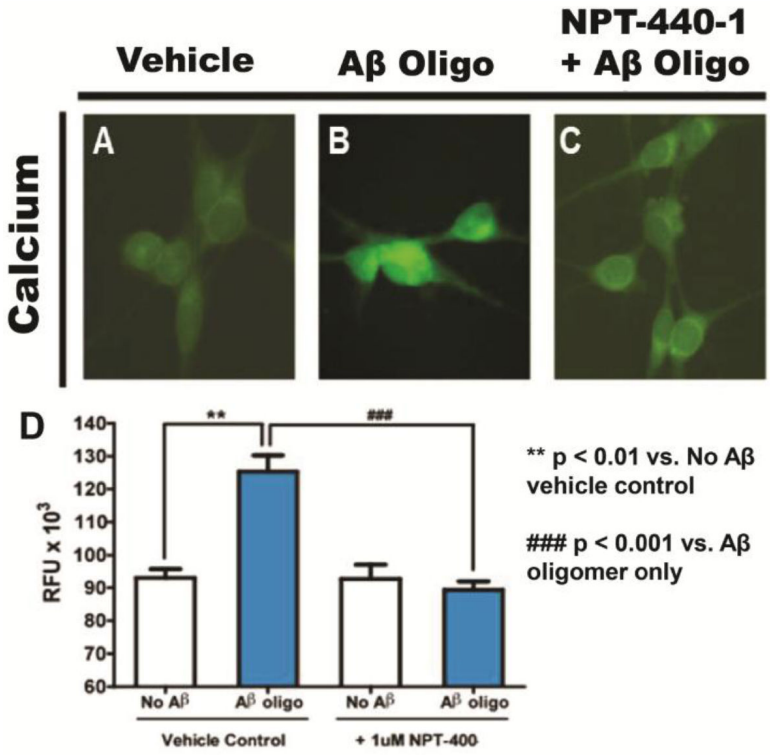

FIGURE 2. $A\beta_{1-42}$ oligomer-induced intracellular Ca^{2+} increases are normalized by NPT-440-1

B103 rat neuronal cells were incubated for 16 h, followed by Fluo-4 MW Calcium imaging studies under the following conditions: **A)** No Aβ vehicle control; **B)** 1 μM oligomerized $A\beta_{1-42}$; **C)** 1:1 co-incubation of oligomerized $A\beta_{1-42}$ with NPT-440-1. **D)** Quantification of fluorescence intensity measured from **A–C**. A significant increase ($p < 0.01$) of intracellular Ca^{2+} was induced by $A\beta_{1-42}$. Addition of NPT-440-1 during incubation with $A\beta_{1-42}$ prevented this increase and Ca^{2+} levels remained comparable to the vehicle control.

Author Manuscript Author Manuscript Author Manuscript Author Manuscript

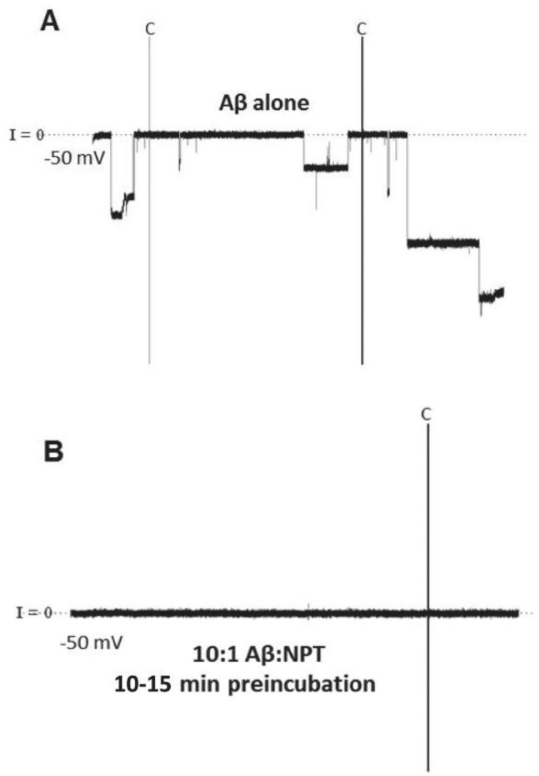

FIGURE 3. NPT-440-1 prevents $A\beta_{1-42}$ pore electrical activity

A) $A\beta_{1-42}$ alone shows multi-level conductance behavior characteristic of amyloid peptides; **B)** 10:1 $A\beta_{1-42}$:NPT-440-1 preincubated 10-15 min prior to addition into the PLB recording chamber showed no pore activity for 4+ h of recording (Figure S1). Inset: High-resolution AFM images of observed pore structures in DOPS/POPE (1:1) membranes. $A\beta_{1-42}$ preincubation with NPT-440-1 does not prevent the formation of pore structures but does inhibit ionic conduction. Conformational change is likely induced within the peptide during preincubation with NPT-440-1, leading to non-conducting pores that are collapsed within the membrane.

Author Manuscript Author Manuscript Author Manuscript Author Manuscript

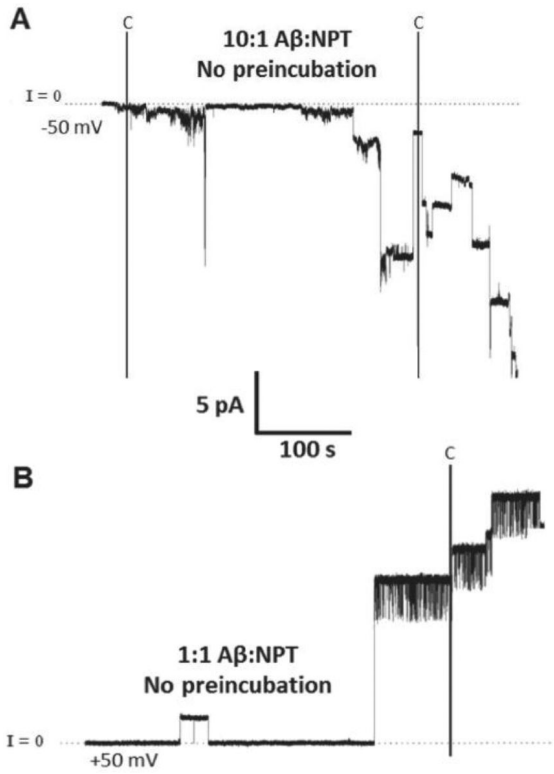

FIGURE 4. Preincubation prior to membrane introduction is necessary to prevent pore activity

A) 10:1 peptide:compound ratio without preincubation shows similar pore activity as $A\beta_{1\text{-}42}$ alone; **B)** 1:1 without preincubation also shows similar pore activity. The need for preincubation prior to membrane introduction implies relatively fast binding and/or insertion of $A\beta_{1\text{-}42}$ into the membrane where it is shielded from the effects of NPT-440-1.

Author Manuscript Author Manuscript Author Manuscript Author Manuscript

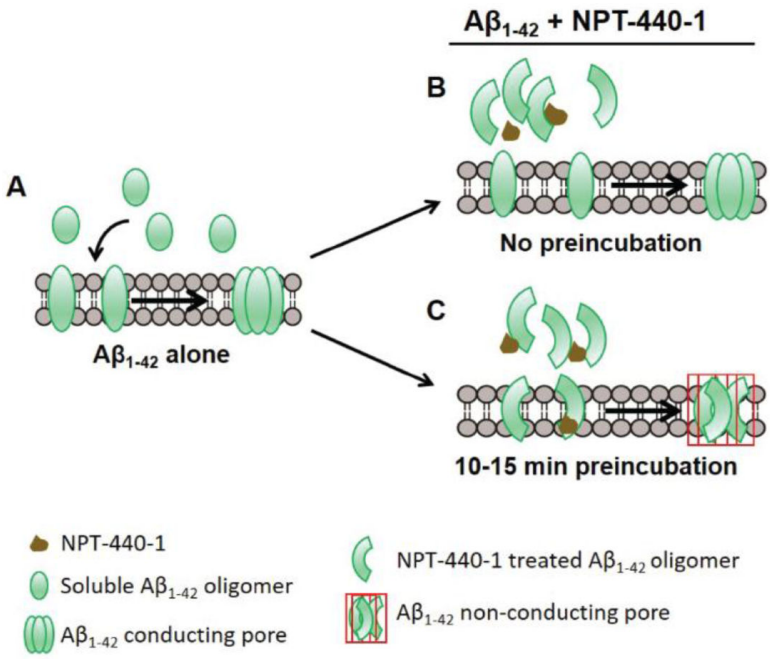

FIGURE 5. Schematic of $A\beta_{1-42}$ interaction with NPT-440-1 and the lipid bilayer

A) Soluble $A\beta_{1-42}$ oligomers insert into the membrane and form pores composed of variable numbers of mobile subunits. The variable nature of these pores leads to heterogenous conductance levels. **B)** Without preincubation, treatment of $A\beta_{1-42}$ with NPT-440-1 has no effect on conductive activity. At least a minor fraction of the $A\beta_{1-42}$ subunits likely insert quickly into the lipid bilayer where they are shielded from the effect of NPT-440-1 and remain free to assemble into conducting pores. **C)** Preincubation of $A\beta_{1-42}$ with NPT-440-1 before addition to the recording chamber allows sufficient time for an induced conformational change, leading to non-conducting/collapsed pores and inhibition of all electrical activity.

Author Manuscript Author Manuscript Author Manuscript Author Manuscript

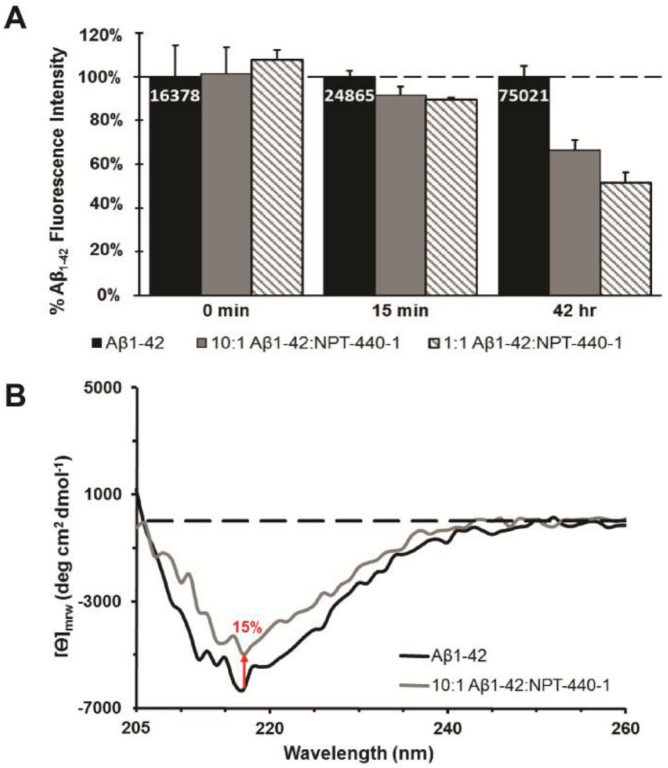

FIGURE 6. Incubation of $A\beta_{1-42}$ with NPT-440-1 reduces β-sheet content

A) ThT fluorescence indicates a concentration-dependent inhibitory effect of NPT-440-1 on $A\beta_{1-42}$ aggregation. Plots have been normalized to the absolute $A\beta_{1-42}$ fluorescence intensity—value shown in white and scaled as 100% (black)—for each time point. Within the first 15 minutes a significant reduction in ThT intensity is measured at both 10:1 (grey, $p < 0.05$) and 1:1 (striped, $p < 0.001$) $A\beta_{1-42}$:NPT-440-1 ratios. Reduction is further enhanced over time and by 42 h the 10:1 and 1:1 signals reach 66.5% and 51.4% of the maximum $A\beta_{1-42}$ ThT intensity respectively ($p < 0.001$). **B)** The CD spectrum of $A\beta_{1-42}$ (black) shows β-sheet rich secondary structure with a characteristic negative peak near 218 nm. 10:1 treatment with NPT-440-1 (grey) shows an upward shift of the spectrum and a 15% reduction in signal at 218 nm (red arrow) indicating a reduction in $A\beta_{1-42}$ β-sheet content after 15 min of incubation. The spectra are expressed as mean residue ellipicity ($[\theta]_{mrw}$) in deg cm^2 $dmol^{-1}$.